

MICROSTRUCTURAL CHARACTERISTICS, MECHANICAL AND WEAR BEHAVIOUR OF ALUMINIUM-ALLOYED DUCTILE IRONS SUBJECTED TO TWO AUSTEMPERING PROCESSES

ABDULLAHI OLAWALE ADEBAYO^{a,b,*}, AKINLABI OYETUNJI^b,
KENNETH KENAYO ALANEME^{b,c}

^a Federal University Oye-Ekiti, Faculty of Engineering, Department of Materials and Metallurgical Engineering, Oye-Are Road, 371101 Oye-Ekiti, Ekiti, Nigeria

^b Federal University of Technology Akure, School of Engineering and Engineering Technology, Department of Metallurgical and Materials Engineering, PMB 704, 340001 Akure, Ondo, Nigeria

^c University of Johannesburg, Faculty of Mining, Metallurgy and Chemical Engineering, Center for Nanoengineering and Tribocorrosion, Cnr Siemert and Beit Street, 2094 Doornfontein, South Africa

* corresponding author: abdullahi.adebayo@fuoye.edu.ng

ABSTRACT. The effect of aluminium addition and austempering processes on the microstructures, mechanical and wear properties of rotary melting furnace processed ductile irons was investigated. Ductile irons containing 1 – 4 wt.% Al were produced and subjected to single and two-step austempering processes. Optical microscopy was used to characterize the graphite features and estimate the volume fraction of the matrix phases present, while the x-ray diffractogram was also carried out to analyse the samples. Mechanical and wear properties of the alloys were equally evaluated. From the results, it was observed that both the as-cast and austempered ductile iron microstructures contained nodular graphite, and the matrix structure for the as-cast ductile irons consisted predominantly of pearlite and ferrite, while that of the austempered grades, contained principally, ausferrite. The microstructure and intermetallic compound obtained played dominant role on the properties of the alloys. The aluminium addition and austempering processes had a significant influence on the mechanical properties and wear resistance of the alloys. The austempered ductile irons exhibited superior strength and wear resistance compared to the as-cast samples, albeit ductility values were lower in the composition group. Austempering increased the strength by over 100% while the addition of Al further enhanced the strength. The improved properties were linked to the refined microstructure, increased proportion of ausferrite phase and intermetallic compound formed. For all properties evaluated, the two-step austempering yielded better properties combination than the single step process. The rotary melting furnace processing adopted was found viable for ductile iron production.

KEYWORDS: Al-alloyed ductile iron, spheroidization, graphite nodules, ausferrite, mechanical properties, wear.

1. INTRODUCTION

There is a growing interest in the development of Al-alloyed ductile irons because of the potential cost, microstructural and property benefits accruable through its use as alloying addition. Al is a relatively cheap and readily accessible metallic material and its use in the development of Al-alloyed ductile irons have been found applicable in automobile component design. The use of Al as alloying addition in ductile irons has been reported to have the potentials of improving machinability, high strength and good toughness, improved fatigue and wear resistance, as well as enhanced heat and fire resistance [1–6]. The improved properties are achieved because Al is a graphitizer and acts by increasing the eutectoid temperature of cast irons, thereby increasing the allowable working temperature [1, 5, 7, 8]. It has also been reported that it influences significantly the form, size and distribution of graphite in ductile iron microstructures. However,

its presence in cast iron melt hinders spheroidization of graphite, which can ultimately affect the overall properties of the “ductile iron” produced, most especially, through sand mould casting. The counteracting effect of aluminium on achieving nodularity has been attributed to its impact in widening the eutectic temperature of cast irons and a lower cooling rate, giving sufficient time for some growing nodules to come in contact with/impinge on adjacent nodules, which eventually distorts their morphology, leading to loss in sphericity [9]. Despite the seeming undesirable effect of Al on crystallization of nodular graphite, a proper process control has since been identified as a key to harnessing the most desirable graphite morphologies possible. Process control in this context applies to factors, such as melting furnace, selected melt practices, modus of inoculation, among others [9–11].

Evidence from literature shows that the most common melting furnaces used for ductile iron produc-

Elements	Weight percent(wt.%)
Fe	93.736
C	3.092
Si	1.522
Mn	0.749
S	0.033
P	0.05
Cr	0.378
Ni	0.137
Al	0.00148
Cu	0.149
Ti	0.036
V	0.03
W	0.0001
Nb	0.0001
Mo	0.071
B	0.002

TABLE 1. Composition of cast iron sleeve scraps used for the production of the Al-alloyed ductile iron (wt.%).

tion are induction, gas-fired crucible, and vacuum furnaces [9, 10, 12–14]. Very little has been reported on the use of rotary melting furnace technology for the production of Al-alloyed ductile irons. Rotary melting furnace is a much cheaper and operationally more flexible furnace type, easier to acquire by small and medium scale foundries for ductile iron production [15]. If applicable, it can help to increase the ductile iron production by small and medium scale foundry enterprises. The present study has been designed to study the effect of Al alloying and austempering (single and two-step) processes on ductile irons that are produced through the use of rotary melting furnace processing. The research questions which this study intends to provide answers to are: Is it possible to deploy rotary melting furnace processing for the production of Al-alloyed ductile irons? Can austempering process be adopted to enhance the mechanical and wear properties of the ductile irons? Are these properties sensitive to the type of austempering schedule utilized? Which compositions of the Al-alloyed ductile irons yield the best combination of mechanical and wear properties? It is expected that the research outcomes from the investigations will provide scientific and technical insights to the desirability or otherwise of rotary furnace melting and austempering treatment for the processing of Al-alloyed ductile irons.

2. MATERIALS AND METHODS

2.1. MATERIALS

The materials used in the research include the following: engine sleeve scraps of cast iron that is free from rust, oil, grease and hydrocarbon materials, aluminium ingot (98.64% grade), 66% grade of graphite, ferro-silicon-FeSi alloy (72.5% analytical grade) in

lumps and powders, and ferro-silicon-magnesium FeSiMg alloy (5.2%). The chemical compositions of the engine sleeve cast iron scraps and the alloying additions are presented in Tables 1 and 2.

2.2. AL-ALLOYED DUCTILE IRONS PRODUCTION

In order to achieve the expected alloy compositions, Equations 1 and 2 were used in the charge calculations. These are in an accordance with [7, 16, 17]. The charge composition was carefully formulated with little quantity of aluminium (Al) in an amount that will ensure a formation of solid solution and which will not attract oxygen intake at that high temperature of the melt. The humidity of the sand mould was also ensured appropriate and with suitable permeability of the mould to allow escape of gases that might be entrapped. It is worthy to note that in a rotary furnace process, the oxidizing flame that brings the charge to the required temperature is in a direct contact with the melt. This often results in high carbon and other elemental constituent losses during melting. Hence, adequate consideration was given to this possibility with the addition of an appropriate compensation percentage of these constituents in order to balance the charge composition [18].

$$\begin{aligned} \text{Amount in base metal/scrap} &= \\ &= \frac{\text{Element in the scrap} \times \text{Quantity charged}}{\text{Furnace capacity}} \quad (1) \end{aligned}$$

$$\begin{aligned} \left(\begin{array}{c} \text{Amount of alloying} \\ \text{element to be added} \end{array} \right) &= \quad (2) \\ &= \frac{\left(\begin{array}{c} \text{Required} \\ \text{amount} \end{array} \right) - \left(\begin{array}{c} \text{Amount in} \\ \text{the base} \\ \text{metal} \end{array} \right) \times \left(\begin{array}{c} \text{Total wt.} \\ \text{of the} \\ \text{charge} \end{array} \right)}{\text{Purity of the alloying element}} \end{aligned}$$

For the study, four different batches of melt charge materials were prepared based on the charge calculations. They were subsequently charged into the furnace, which was pre-heated to 1300 °C. The continuous rotary motion of the furnace helped to enhance a uniform distribution of the heat in the furnace and homogenization of the melt composition. The aluminium ingots to be used for the alloying, were also pre-heated to 450 °C, and then charged into a pre-heated ladle that contained the nodularizing agent enclosed within the ladle, ready for melt discharge from the rotary furnace. The enclosure of the nodularizing agent from immediate direct melt contact helps facilitate the spheroidization process, by delaying the reaction of the melt with the nodularizer (FeSiMg) in the ladle, which reduces the rate of burn off (fading) of the very reactive magnesium. The nodularization reaction at the base pocket of the ladle was allowed

		Materials		
		ZFSB-5 (MgFeSi)	FeSi	Graphite
Elemental composition (%)	Si	42 – 44	72.5	–
	Mg	4.8 – 5.2		–
	Ca	Moderate		–
	RE	0.8 – 1.2	1.75	–
	Sb	Moderate		–
	Al	< 1.0	1	–
	Fe	Bal.	Bal.	–
	Cu		1	–
	C			66.0
	Ash		–	30.2
	S		–	0.57
	Moist		–	0.10
	VM		–	3.10

TABLE 2. Compositions of the nodularizer (FeSiMg), FeSi and graphite used for treating the cast iron melt.

to take place for 48-50 seconds followed by melt de-slagging in 90 second at a temperature of 1430 °C. The ladle was brought very close to the mould's sprue to avoid turbulent pouring, which can entrap oxygen and hydrogen intake; and subsequently poured the nodularized melt at about 1350 °C gently into the prepared sand mould. The mould cavity has a reaction chamber containing ferro-silicon alloy, for in-mould inoculation of the melt before solidification of the cast. This process facilitates spontaneous and effective nucleation of the melt during solidification. The casts were allowed to cool in the mould, and afterwards, knocked out, fettled and machined into various tests samples.

2.3. AUSTEMPERING OF THE AL-ALLOYED DUCTILE IRONS

The samples for the austempering were preliminarily subjected to normalizing at 800 °C. Thereafter, the samples for the single step austempering were austenitized and homogenized at a temperature of 850 °C for 90 minutes, and then quenched in a molten salt bath (50 % KNO₃:50 % NaNO₃) maintained at 400 °C for 90 minutes for isothermal transformation into ausferrite. Afterwards, the samples were cooled by air. In the case of the two-step process, the samples were austenitized and homogenized at a temperature of 850 °C for 90 minutes, then quenched in a molten salt bath maintained at 260 °C for 5 minutes, intended to achieve partial isothermal transformation of austenite into fine-grained ausferrite. The samples were swiftly transferred to another salt bath maintained at 400 °C for 90 minutes, to achieve complete transformation of austenite to ausferrite [19]. The samples were equally cooled in air after the austempering treatment.

2.4. ELEMENTAL ANALYSES

The quantitative estimation of the chemical compositions of the Al-alloyed ductile irons produced was carried out with an arc-spectrometer of model 2000-3

Spetro-CJRO. The sample for the test was mounted on the sparking point of the spectrometer machine after each sample surface had been prepared. Each of the samples was sparked three (3) times, the mean value taken, and the results of the chemical composition read on the monitor of the machine. Equation 3 was thereafter used to obtain the carbon equivalent values (CEV) of the ductile irons.

$$\text{CEV} = \% \text{C} + 0.3 \% \text{Si} + 0.33 \% \text{P} - 0.027 \% \text{Mn} + 0.4 \% \text{S} + 0.125 \% \text{Al} \quad (3)$$

where: % C, % Si, % P, % Mn, % S and % Al are the percentages of carbon, silicon, phosphorous, manganese, sulphur and aluminium, respectively. The chemical composition and carbon equivalent of the ductile irons produced are presented in Table 3.

2.5. MICROSTRUCTURAL CHARACTERIZATION

The metallographic examination of the samples obtained from the as-cast and austempered ductile irons was carried out using an optical metallurgical microscope of model Axio-observer A1m equipped with Axio-Cam ERc5 camera for image capturing. Emery papers of grades 120, 220, 400, 600 and 800 grits were used for sample surface grinding; after which the samples were polished using 1000 and 1200 grits; and diamond polish suspension of 3 microns to achieve a mirror surface finish. Etching of the polished samples was performed using 2 % nital solution, by swabbing the samples for two minutes before the microstructural examination was performed [20]. The XRD was also carried out using PW1710 Philips diffractometer with monochromatic Cu target K- α radiation at 40 kV and 45 mA equipped with a high score X'Pert software. The operational condition was selected to obtain x-ray diffraction diagrams of sufficient counting statistics, narrow peaks. X-ray data were collected over a 2Theta (2θ) range of 24.0915 – 85.6744° with

a step size of 0.017°. Planimetric method of visual analysis was used to characterize the graphite morphology of the ductile irons, while the microstructural features were analysed using a computer aided image analysis software equipped to the optical microscope. The microstructural analysis was done in accordance with ISO classifications for ductile and vermicular cast irons in as-cast and austempered state [21–23].

2.6. MECHANICAL TESTING

Mechanical testing of both the as-cast and austempered Al-alloyed ductile irons was performed to evaluate their mechanical properties. The micro-hardness values of the ductile irons were determined with the aid of micro-hardness vickers tester of model FALCON 500 series having a diamond indenter. An applied load of 100 gf and dwelling time of 15 seconds was adopted for the test, which was performed on the polished surface of the samples. A mean of five measurements for each sample was taken in line with [24] standard for the determination of the hardness. A table-top universal tensiometer of model KPL 2000-1 with self-aligned Instron 8800 digital controlled panel was used to perform tension tests on the ductile irons produced. Three tensile test samples with gauge length of 28 mm and gauge diameter of 7 mm were machined for each ductile iron composition and the tests were carried out in an accordance with [25]. The mean values of results were evaluated to determine the ultimate tensile strength and % elongation of the ductile irons.

2.7. WEAR TESTING

The behaviour of the ductile irons samples under wear were evaluated on dry sliding environment at room temperature of 25 °C to determine the wear resistance using ROTOPOL V product, a pin-on-disk type machine to perform the test. After measuring the initial weight of the sample, the test was carried out by firmly mounting the (10 × 10 × 50) mm sample parallel to the surface of the rotating disc of the wear testing machine at 25 cm radius. A grit size of 220 was used for the test with a revolution rate of 150 rpm. A load of 5N was applied for a period of five (5) minutes in accordance with [26] as expressed in the work of [27]. The surface of the sample was cleaned with cotton wool and the final weight taken. The wear resistance was computed using Archard's expressions in equations 4 to 6 [28].

$$\text{Wear rate} = \frac{\text{Wear volume}}{\text{Load} \times \text{Sliding distance}} \quad (4)$$

$$\text{Sliding distance} = 2 wtl \times R \quad (5)$$

where wtl is the wear track length and R is number of revolution or frequency

$$\text{Wear resistance} = \frac{1}{\text{Wear rate}} \quad (6)$$

Elements	Melt 1	Melt 2	Melt 3	Melt 4
C	3.541	3.527	3.411	3.408
Si	2.92	2.21	2.09	2.01
Al	0.024	2.29	3.02	3.74
Mn	0.40	0.377	0.372	0.381
P	0.073	0.062	0.074	0.068
S	0.025	0.018	0.013	0.01
Cr	0.102	0.109	0.102	0.103
Cu	0.121	0.135	0.138	0.134
Mg	0.071	0.076	0.046	0.049
Ca	0.0027	0.0017	0.0012	0.0014
Fe	Bal.	Bal.	Bal.	Bal.
C.E.	4.443	4.494	4.436	4.495

TABLE 3. Chemical composition of the alloys produced.

3. RESULTS AND DISCUSSIONS

3.1. CHEMICAL COMPOSITION OF THE AL-ALLOYED DUCTILE IRONS

The results of the spectrographic analyses performed on the Al-alloyed ductile irons are presented in Table 3. It is observed that all the ductile irons (melts 1-4) produced have carbon equivalent (CE) values above 4.3. This implies that the ductile irons produced are hyper-eutectic in composition and thus should have a hyper-eutectic structure. As expected, the higher the CE value, the higher the tendency of carbon to precipitate as graphite cooling from the liquid state to the eutectic temperature [29].

3.2. MICROSTRUCTURAL CHARACTERIZATION OF THE AL-ALLOYED DUCTILE IRONS

Figs. 1 to 4 present the optical micrographs of the Al-alloyed ductile irons produced. It is noted that both the as-cast and austempered ductile iron microstructures contain nodular graphite. The as-cast ductile iron matrices consist of predominantly pearlite and ferrite while that of the austempered grades, contained principally, ausferrite. The microstructural features observed are typical of features in ductile irons produced using conventional melting furnaces and inoculation procedures [10, 11, 30]. This suggests that the rotary melting furnace adopted is viable for a ductile iron production. Also, from the microstructural features observed in the micrographs of the ductile irons, it is apparent that the Al addition and austempering processes resulted in significant changes in the microstructure of the ductile irons. These microstructural features were qualitatively and quantitatively analysed and the results summarized in Table 4.

From the Table 4, it is observed that the effect of Al was more consistent on the nodule count, which is observed to increase with the increase in Al wt.%. The matrix structure of the as-cast ductile irons consists of pearlite and ferrite, which only showed higher pearlite content (than the ductile iron composition without Al) for the compositions containing 3.02 and 3.74

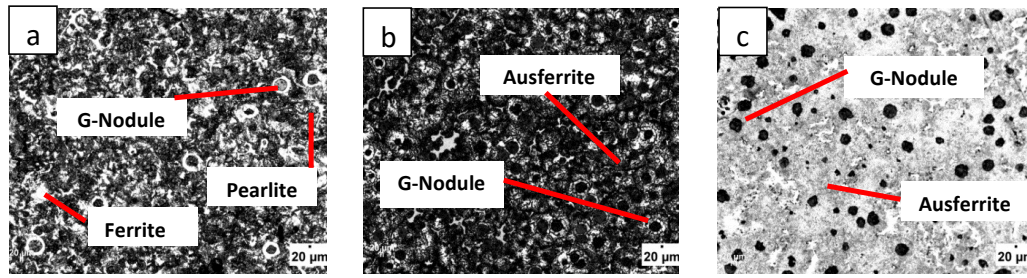


FIGURE 1. Optical micrographs of as-cast ductile iron (a) Without austempering (b) Austenitized at 850 °C and austempered at 400 °C for 90 min [conventional austempering] (c) Austenitized at 850 °C, austempered at 260 °C for 5 min. and 400 °C for 90 min. [two-step austempering]

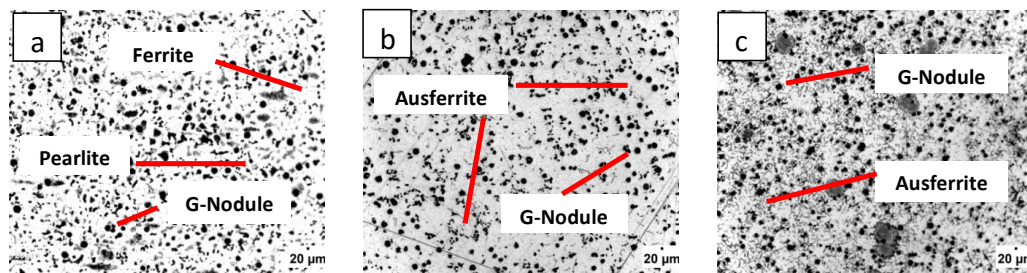


FIGURE 2. Optical micrographs of 2.29 wt.% Al-alloyed ductile iron (a) Without austempering (b) Conventional austempering (c) Two-step austempering.

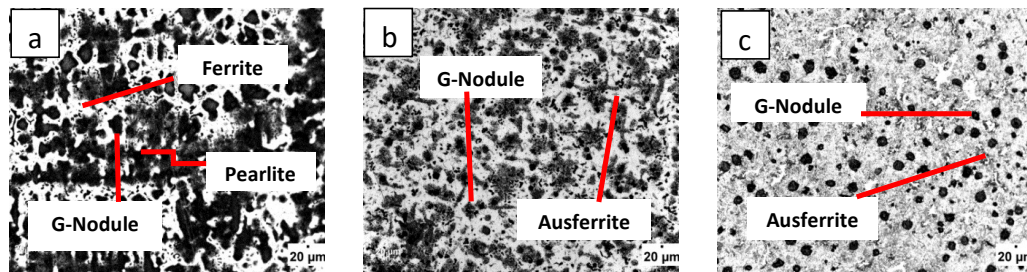


FIGURE 3. Optical micrographs of 3.02 wt.% Al-alloyed ductile iron (a) Without austempering (b) Conventional austempering (c) Two-step austempering.

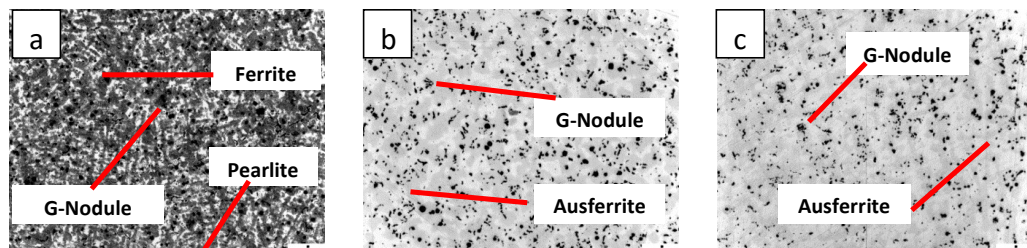


FIGURE 4. Optical micrographs of 3.74 wt.% Al-alloyed ductile iron (a) Without austempering (b) Conventional austempering (c) Two-step austempering.

Alloy	Heat treatment process	Form of G-precipitate	Characteristics of G-precipitate	Nodule counts (mm ⁻²)	% nodule volume fraction	% phases (volume fraction) A - ausferrite, α -Fe – ferrite, P – pearlite
Without Al	As-cast	VI, V, IV	35 % VI 6, 15 % VI 7, 10 % V 6, 10 % V 7, 15 % IV 7, 15 % IV 8	188	11.62	% α -Fe: 33.80 %P: 54.58
Without Al	A γ 850/400 °C	VI, V, IV, III	35 % VI 6, 20 % V 6, 30 % IV 8, 15 % III 7	222	13.27	%A: 86.73
Without Al	B 850/260/400 °C	VI, V	50 % VI 6, 20 % V 6, 20 % VI 7, 10 % V 8	270	14.26	%A: 85.74
2.29 wt.% Al	As-cast	VI, V, IV, III	25 % VI 7, 30 % V 8, 30 % IV 8, 15 % III 6	536	13.23	% α -Fe: 58.69 %P: 28.08
2.29 wt.% Al	A γ 850/400 °C	VI, V, IV, III	5 % VI 8, 25 % V 8, 50 % IV 7, 20 % III 6	844	9.24	%A: 90.76
2.29 wt.% Al	B 850/260/400 °C	VI, V, IV, III	60 % VI 8, 20 % V 8, 10 % IV 7, 10 % III 7	872	12.54	%A: 87.46
3.02 wt.% Al	As-cast	VI, V, IV, III	65 % III 6, 15 % IV 7, 10 % VI 7, 10 % V 7	468	10.15	% α -Fe: 33.91 %P: 55.95
3.02 wt.% Al	A γ 850/400 °C	VI, V, IV, III	50 % IV 8, 20 % III 7, 15 % VI 8, 15 % III 6	726	8.70	%A: 91.3
3.02 wt.% Al	B 850/260/400 °C	VI, V, IV, III	40 % VI 7, 35 % V 8, 20 % IV 7, 5 % III 7	512	10.87	%A: 89.13
3.74 wt.% Al	As-cast	VI, V, IV, III	40 % IV 7, 20 % III 6, 25 % VI 6, 15 % V 6	780	10.35	% α -Fe: 23.25 %P: 66.40
3.74 wt.% Al	A γ 850/400 °C	VI, V, IV, III	35 % IV 6, 45 % III 6, 10 % VI 7, 10 % V 7	852	5.23	%A: 94.77
3.74 wt.% Al	B 850/260/400 °C	VI, V, IV, III	10 % VI 8, 10 % V 8, 15 % IV 8, 65 % III-7	464	5.26	%A: 94.74

TABLE 4. Features of micrographs of the Al-alloyed ductile irons in as-cast and austempered conditions.

wt.% Al. The same compositions also exhibited the least nodularity judging from their relatively lower volume fraction of graphite nodules (10.15 and 10.35 %, respectively). This phenomenon of reduced sphericity has been associated with an increased Al wt.% and a postulation to explain the reason, linked it to the tendency of Al to absorb oxygen at the graphite surface, which interferes with the growth into perfect spheroid by reducing the rate of the carbon diffusion [30].

Also from the Table 4 (which compares the microstructural parameters of the as-cast and austempered ductile irons), it is observed that the austempering process affected the % volume fraction and matrix structure of the austenite. The process resulted in a matrix structure consisting predominantly of a mixture of carbon-stabilized austenite and acicular ferrite (ausferrite) which is in contrast with the as-cast ductile irons that had a pearlite-ferrite matrix structure. The acicular ferrites are the dark needle-like structures while the carbon-stabilized austenite being the white regions. However, some microstructural differences were observed in the case of these austempered Al-alloyed ductile irons. There seemed to be inhomogeneity rather than the usual blocky matrix structure. Also, the packets and groups of needles were shorter and fragmented. The inhomogeneity that characterized the ausferrite morphology

may be due to the micro-segregation effect in the ferrite and retained austenite comprising the ausferrite. It could also be due to an incomplete reaction in the entire austenite which remains untransformed in the microstructure [31–33]. For most of the compositions, the results of the image analysis used to estimate the volume fractions of the phases revealed that the single step austempering process yielded slightly higher ausferrite content compared with the two step austempering process.

The representative x-ray diffractograms of the 2.29 wt.% Al-ductile irons in as-cast and austempered conditions are presented in Figures 5-7. The profiles, which were analysed using a high score X'Pert software, indicated the peak positions, identified pattern lists and sets of miller indices (011, 002, 112), (111, 022, 113, 222, 004) and (111, 002, 022, 113, 222). From the sets of diffracting crystal planes, BCC (body centred cubic) ferrite and its mixture with FCC (face centred cubic) were confirmed. This suggests that pearlite, a mixture of ferrite and cementite, is found as phases in the as-cast ductile irons, while the phases are in form of ausferrite for the austempered samples. Aside the two foremost phases of ferrite, cementite and/or their mixture as pearlite, formation of intermetallic compounds were also observed in the as-cast and austempered pattern. The as-cast samples re-

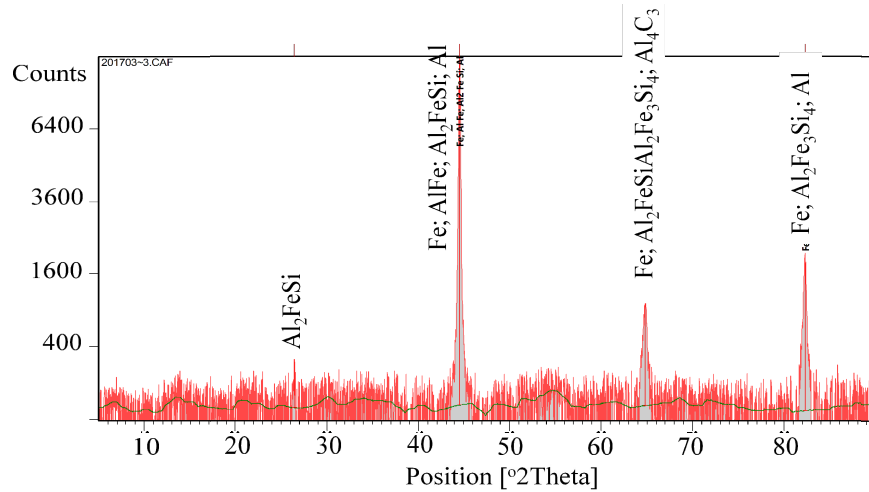


FIGURE 5. Intensity (counts) against 2 theta (degree) of 2.29 wt.% Al-alloyed ductile iron produced.

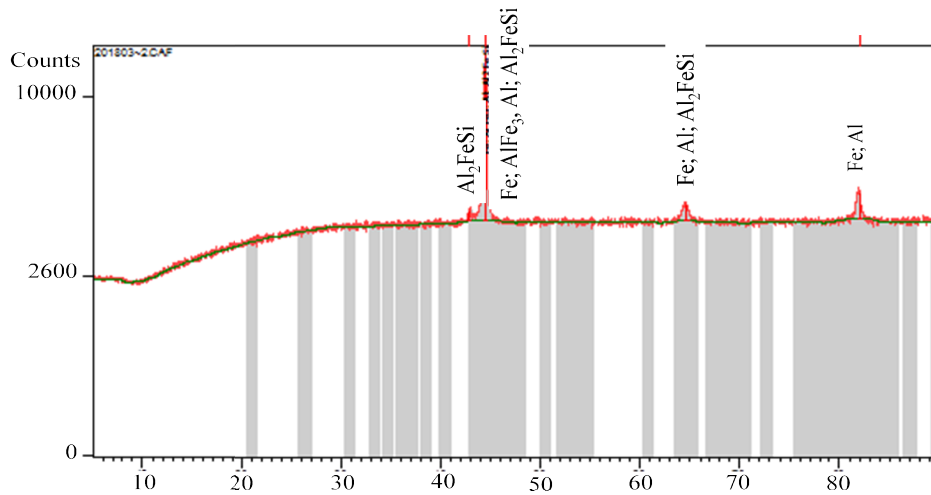


FIGURE 6. Intensity (counts) against 2 theta (degree) of 2.29 wt.% Al-alloyed ductile iron austenitized at 850 °C and Austempered at 400 °C for 90 min.

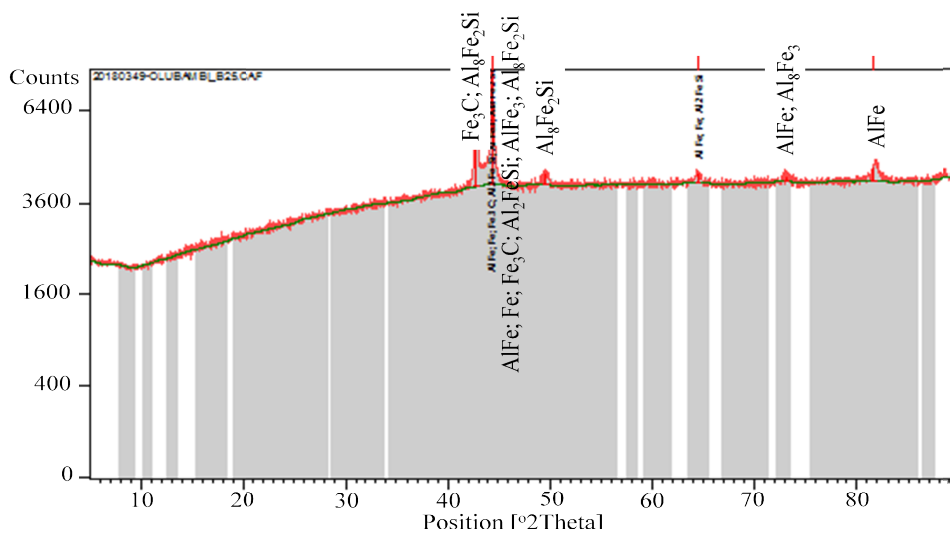


FIGURE 7. Intensity (counts) against 2 theta (degree) of 2.29 wt.% Al-alloyed ductile iron austenitized at 850 °C and Austempered at 260 °C for 5 min. and 400 °C for 90 min.

vealed compound, such as Aluminium-Silicon-Carbide (Al_4SiC_4), Magnesium-Silicon (Mg_2Si), Aluminium-Iron-Silicon ($\text{Al}_2\text{Fe}_3\text{Si}_4$ and Al_5FeSi), Aluminium-Carbide (Al_4C_3) and Aluminium-Iron (AlFe). However, when austempered, these compounds: Ferrite (Fe), Ferro-silicite (FeSi), Magnesium-Silicon (Mg_2Si), Aluminium-Iron (AlFe , AlFe_3), Aluminium-Iron-Silicon (Al_2FeSi , Al_8FeSi), Cementite (Fe_3C), Iron-Carbide (Fe_2C), and Magnesium-Aluminium-Carbide (MgAl_2C_2) were found. The phases identified in the ductile irons produced are principally in an agreement with that reported by Palm (2005) [34] and Connetable et al. (2008) [35].

3.3. MECHANICAL PROPERTIES OF THE AS-CAST AND AUSTEMPERED ALLOYS PRODUCED

Figs. 8-11 present the results of the mechanical tests performed on the as-cast and austempered Al-alloyed ductile irons. The microstructure obtained is the dominant factor for the increase in the tensile strength. The strengthening effect could be ascribed to the formation of aluminium solid solution, which was equally amplified by the grain boundary effect due to grain sizes refinement. The more the precipitates, the more the strength increases. The isothermal transformation (austempering) led to the production of fine phases of ferrite and carbon stabilized austenite microstructure (ausferrite) with finer sizes of nodules embedded in the matrices. The fine graphite precipitates observed in the matrices enhance the strength of the ductile irons. The formation of intermetallic compounds (Figs. 5-7) within the matrix structure also contributes to particle strengthening by the Orowan mechanism by serving as additional barriers to the motion of dislocations, hence, playing a key role in the increase of the strength [3, 8, 11, 36-39].

Fig. 8, which presents the hardness results of the ductile irons, shows that the hardness values increase with an increase in Al wt.% in the as-cast ductile irons. The hardness increased from a value of 282.29 $\text{HV}_{0.1}$ for the ductile iron without Al to 412.79 $\text{HV}_{0.1}$ for the composition containing 3.74 wt.% Al. The increased hardness observed in the Al containing ductile iron compositions is accounted to the grain refining effect the Al induces on the microstructure and also the relatively enhanced pearlite content, particularly for the 3.02 and 3.74 wt.% Al containing ductile iron compositions. Thus, the increased hardness can be linked to grain boundary and phase strengthening. For the austempered ductile irons, it is observed that single step austempering resulted in only marginal increase in hardness for the compositions containing up to 2.29 wt.% Al. The hardening effect of the single step austempering was, however, more significant for the ductile iron compositions containing 3.02 and 3.74 wt.% Al. For the two-step austempered ductile irons, hardness improvement was observed for all ductile iron compositions, and the hardness values were

consistently the highest for all the processed conditions evaluated (that is, as-cast, single step, and two-step austempered conditions). The enhanced hardening observed for the two step austempered structure may be attributed to the improved refinement of the grain structure and ausferrite volume fraction in the ductile irons. The [40] Jeffries' procedure (planimetric) used to estimate the grain size revealed that while the single step processed samples have grain sizes equivalent to ASTM grain size number that ranged from G 1 to G 2.5, the two-step austempered samples ranged between G 1.5 and G 3. Ausferrite is noted to significantly improve the mechanical properties of ductile irons, which is even more remarkable for the two-step austempering process. This is because the finer grains of ausferrite are obtained by nucleation and growth. In the present case, the large super-cooling at a lower temperature (260 °C) facilitates more nuclei formation and/or partial transformation, after which the austempering at a higher temperature (400 °C), ensures the growth and completion of the transformation [32]. Thus, boundary strengthening and phase hardening (ausferrite) are the operational micro-mechanisms that are responsible for the improved hardness.

3.4. TENSILE PROPERTIES

The results of the tensile tests performed on the ductile irons are presented in Fig. 9. It is observed that for the as-cast ductile irons, the tensile strength increases slightly with the increase in Al wt.%. The strength increases are, however, more remarkable for the austempered ductile iron grades with over 100% increase for all the compositions in comparison with the as-cast ductile irons. It is noted that the two-step austempered ductile irons had the highest tensile strength values, albeit the values were marginally lower than that for the single step austempered ductile irons. The remarkable improvement in the tensile strength of the austempered ductile irons can be attributed to the isothermal transformation (austempering), which led to the production of fine phases of ferrite and carbon stabilized austenite microstructure (ausferrite) with finer sizes of nodules embedded in the matrix as can be confirmed from Figs. 1-4. The microstructures, which consist of refined grain size of ausferrite, are the dominant factors for the increase in the tensile strength. However, the inverse effect is observed with respect to ductility (Fig. 10), as the austempered ductile iron grades had significantly reduced ductility compared to the as-cast ductile irons. The effect is observed to be more severe for the single step austempered ductile irons, which had the least ductility values. It has been well-established that for most ferrous alloys, the strength increase is achieved at the expense of ductility - when hardness and strength increase, ductility is lowered. However, in an accordance with [23, 41], the ductility for as-cast and austempered ductile irons is in the range of 19-23% and 7-10%, respectively. In the present study,

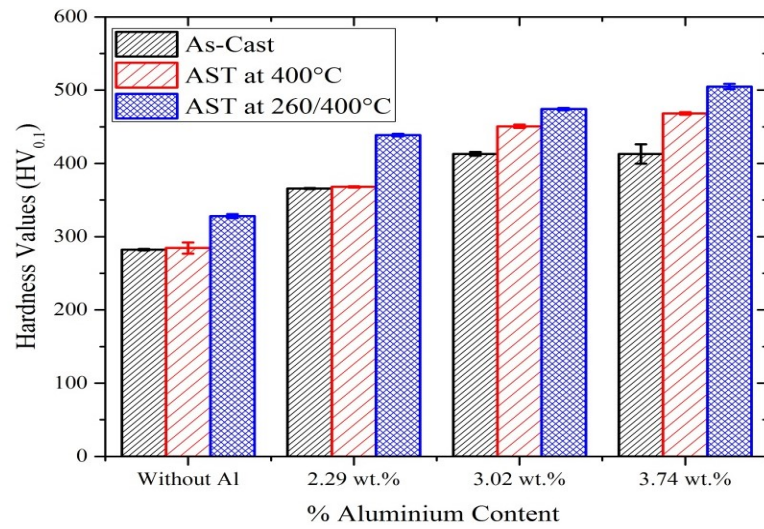


FIGURE 8. Variation of hardness values (HV_{0.1}) with Aluminium (wt.%) in the as-cast and austempered ductile irons produced.

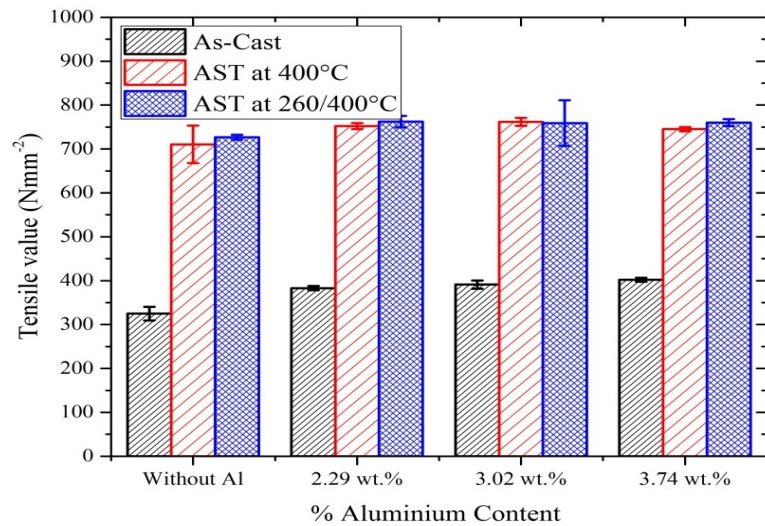


FIGURE 9. Variation of ultimate tensile strength with Aluminium (wt.%) in the as-cast and austempered ductile irons produced.

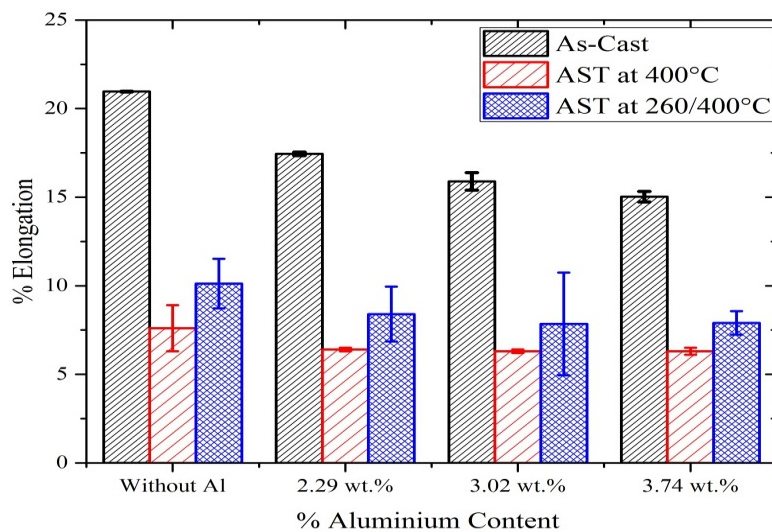


FIGURE 10. Variation of % elongation with Aluminium (wt.%) in the as-cast and austempered ductile irons produced.

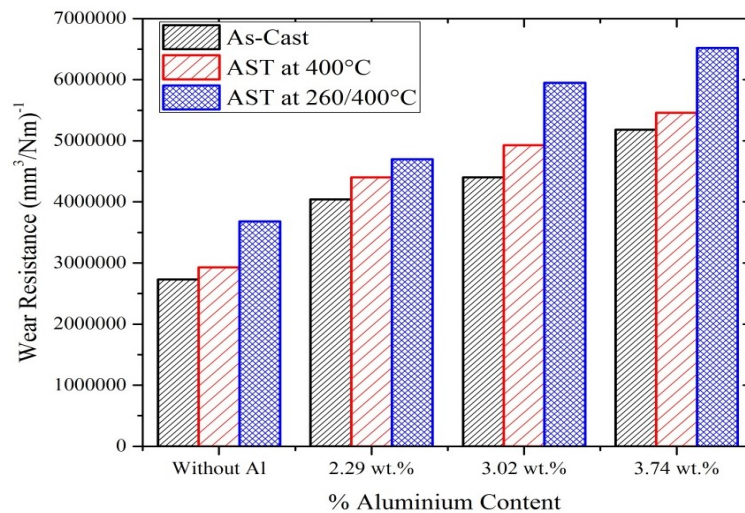


FIGURE 11. Variation of wear resistance ($\text{mm}^3/\text{Nm}^{-1}$) with Aluminium (wt.%) in the as-cast and austempered ductile irons produced.

the ductility values of the Al alloyed ductile irons were in the range 6.3 – 9.35 %, which is still close to the standard values of 7-10 % elongation established for ductile iron without aluminium [23, 37]. Based on the tensile properties, the two step austempered ductile iron compositions containing 2.29 and 3.02 wt.% Al had the best combination of tensile properties of all the processed ductile irons produced.

3.5. WEAR RESISTANCE OF THE ALLOYS

The wear resistance results of the as-cast and austempered Al-alloyed ductile irons are presented in Fig. 11. It is observed that the wear resistance increases with the increase in Al wt.% and was more remarkable for the compositions containing 2.29, 3.02, and 3.74 wt.% Al. It is also observed that the wear resistance improved with austempering of the ductile irons, with the samples subjected to two step austempering, recording the highest wear resistance for each composition of the ductile irons. The initial partial transformation at a lower austempering temperature of 260 °C (initial super-cooling) led to the precipitation of finer grains of ausferrite in the matrix before growth; consequently, this strengthens the microstructure. The improved wear resistance is also influenced due to the formation of intermetallic compound occasioned by the presence of aluminium in the ductile irons as researches have shown that aluminium is one of the elements that improve the strength, hardness and wear resistance of cast irons [5, 8].

4. CONCLUSION

The structural characteristics, mechanical and wear behaviour of Al-alloyed ductile iron subjected to single and double stage austempering processes was investigated in this research. From results, the following conclusions are drawn:

- (1) The rotary melting furnace adopted was found viable for the ductile iron production, as it was noted that both the as-cast and austempered ductile iron microstructures contained nodular graphite, and the matrix structure for the as-cast ductile irons consist predominantly of pearlite and ferrite, while that of the austempered grades, contained principally ausferrite.
- (2) The addition of aluminium improved the nodule count and microstructural properties of the Al-alloyed ductile irons.
- (3) Austempering and Al alloying resulted in an increased hardness and tensile strength values in the ductile irons. The hardness increased with the increase in Al wt.% in the ductile irons, while austempering yielded higher hardness values compared to the as-cast ductile irons. The hardening effect was, however, observed to be more remarkable for the two step austempered ductile iron compositions. The austempered ductile iron grades had significantly reduced ductility compared to the as-cast ductile irons. The effect was observed to be more severe for the single step austempered ductile irons.
- (4) The wear resistance increases with the increase in Al wt.% and it was more remarkable for the compositions containing 2.29, 3.02, and 3.74 wt.% Al. It is also observed that the wear resistance improved with austempering of the ductile irons, with the samples subjected to two step austempering, recording the highest wear resistance for each composition of the ductile irons.

REFERENCES

- [1] M. Soński, P. Kordas, K. Skurka, A. Jakubus. Investigations of ferritic nodular cast iron containing about 5-6% aluminium. *Archives of Foundry Engineering* **16**(4), 2016. DOI:10.1515/afe-2016-0099.

- [2] M. Soiński, A. Jakubus, P. Kordas, K. Skurka. Characteristics of graphite precipitates in aluminium cast iron treated with cerium mixture. *Archives of Foundry Engineering* **15**(1), 2015. DOI:10.1515/afe-2015-0017.
- [3] J. Hampl, T. Elbel, T. Valek. *European Union Metal*. Brno, Czech Republic, 2014.
- [4] S. Shaha, S. Dyuti, H. M.M, M. Maleque. Development of a new route for Fe-C-Al cast iron production. *Journal of Applied Sciences* **10**:1196 – 1199, 2010. DOI:10.3923/jas.2010.1196.1199.
- [5] A. Kiani-Rashid, D. Edmonds. Microstructural characteristics of Al-alloyed austempered ductile irons. *Journal of Alloys and Compounds* **477**(1):391 – 398, 2009. DOI:10.1016/j.jallcom.2008.10.038.
- [6] A. Kiani-Rashid, D. Edmonds. Phase transformation study of aluminium-containing ductile cast irons by dilatometry. *Materials Science and Engineering: A* **481-482**:752 – 756, 2008. Proceedings of the 7th European Symposium on Martensitic Transformations, ESOMAT 2006, DOI:10.1016/j.msea.2007.02.167.
- [7] M. Soiński, J. Góraj. The influence of cerium mixture addition on the structure of cast iron containing about of 5% aluminium. *Archives of Foundry Engineering* **9**:215 – 218, 2009.
- [8] M. Haque, J. Young. Production of spheroidal graphite aluminium cast iron and the factors affecting it. *Journal of Materials Processing Technology* **55**(3):186 – 192, 1995. DOI:10.1016/0924-0136(95)01952-9.
- [9] N. Haghdadi, B. Bazaz, H.-R. Erfanian-Naziftoosi, A. Kiani-Rashid. Microstructural and mechanical characteristics of al-alloyed ductile iron upon casting and annealing. *International Journal of Minerals, Metallurgy, and Materials* **19**(9):812 – 820, 2012. DOI:10.1007/s12613-012-0633-z.
- [10] L. Ceschini, A. Morri, A. Morri. Effects of casting size on microstructure and mechanical properties of spheroidal and compacted graphite cast irons: Experimental results and comparison with international standards. *Journal of Materials Engineering and Performance* **26**(06):2583 – 2592, 2017. DOI:10.1007/s11665-017-2714-7.
- [11] R. Gonzaga. Influence of ferrite and pearlite content on mechanical properties of ductile cast irons. *Materials Science and Engineering: A* **567**:1 – 8, 2013. DOI:10.1016/j.msea.2012.12.089.
- [12] J. Alasoluyi, J. Omotoyinbo, S. Olusunle. Investigation of the mechanical properties of ductile iron produced from hybrid inoculants using rotary furnace. *International Journal of Science and Technology* **2**(5):388 – 393, 2013.
- [13] D. Kopyciński. Effect of Ti, Nb, Cr and B on structure and mechanical properties of high aluminium cast iron. *Archives of Foundry Engineering* **13**(1):77 – 80, 2013. DOI:10.2478/afe-2013-0015.
- [14] M. Zandira, S. M. A. Boutorabi. Fracture characteristics of austempered spheroidal graphite aluminum cast irons. *Journal of Iron and Steel Research, International* **17**(2):31 – 35, 2010. DOI:10.1016/S1006-706X(10)60055-6.
- [15] O. A. Adeyemi, I. M. Momoh, S. S. O. Olusunle, S. Adejuyigbe. Production of ductile iron using indigenously manufactured rotary furnace. *IOSR Journal of Mechanical and Civil Engineering* **11**(5):62–65, 2014. DOI:10.9790/1684-11516265.
- [16] E. Ziókowski, R. Wrona. Using fuzzy optimisation method in calculation of charge burden to correct the chemical composition of metal melt. *Archives of Foundry Engineering* **7**(3):183 – 186, 2007.
- [17] A. Oyetunji, A. Opaluwa. Model development for estimating the aging behaviors of gray cast iron (GCI) alloy at different times and temperatures. *The International Journal of Advanced Manufacturing Technology* **96**(1):705 – 715, 2018. DOI:10.1007/s00170-018-1587-8.
- [18] J. O. Alasoluyi, J. A. Omotoyinbo, J. O. Borode, et al. Influence of secondary introduction of carbon and ferrosilicon on the microstructure of rotary furnace produced ductile iron. *International Journal of Science and Technology* **2**(2):211 – 217, 2013.
- [19] J. Yang, S. K. Putatunda. Improvement in strength and toughness of austempered ductile cast iron by a novel two-step austempering process. *Materials & Design* **25**(3):219 – 230, 2004. DOI:10.1016/j.matdes.2003.09.021.
- [20] O. P. Khanna. *Materials Science and Met.* Dhanpat Rail Publication Limited, New Delhi, 2009.
- [21] ISO 945-1 - Microstructure of Cast Iron – Part 1: Graphite Classification by Visual Analysis. Standard, International Organization for Standardization, Geneva, 2008.
- [22] ISO 16112 - Compact (Vermicular) Graphite Cast Irons - Classification. Standard, International Organization for Standardization, Geneva, 2017.
- [23] ISO 17804 - Founding - Ausferritic Spheroidal Graphite Cast Irons – Classification. Standard, International Organization for Standardization, Geneva, 2005.
- [24] ISO 6507-1 - Metallic materials - Vickers hardness test - Part 1: Test Method. Standard, International Organization for Standardization, Geneva, 2018.
- [25] ISO 6892-1 - Metallic Materials- Tensile Testing- Part 1: Method of Test at Room Temperature. Standard, International Organization for Standardization, Geneva, 2016.
- [26] ASTM G99-05 - Standard Test Method for Wear Testing with a Pin-on-Disk Apparatus. Standard, American Society for Testing and Materials, West Conshohocken, 2005.
- [27] A. Vadiraj, S. Tiwari. Effect of silicon on mechanical and wear properties of aluminium-alloyed gray cast iron. *Journal of Materials Engineering and Performance* **23**(8):3001 – 3006, 2014. DOI:10.1007/s11665-014-1040-6.
- [28] J. F. Archard. Contact and rubbing of flat surfaces. *Journal of Applied Physics* **24**(8):981 – 988, 1953. DOI:10.1063/1.1721448.
- [29] S. O. Seidu, I. Riposan. Thermal analysis of inoculated ductile irons. *UPB Science Bulletin, series B* **73**(2):241 – 254, 2011.

- [30] A. Shayesteh-Zeraati, H. Naser-Zoshki, A. R. Kiani-Rashid, M. R. Yousef-Sani. The effect of aluminium content on morphology, size, volume fraction, and number of graphite nodules in ductile cast iron. *Proceedings of the Institution of Mechanical Engineers, Part L: Journal of Materials: Design and Applications* **224**(3):117 – 122, 2010. doi:10.1243/14644207JMDA302.
- [31] P. Sellamuthu, D. G. Harris Samuel, D. Dinakaran, et al. Austempered ductile iron (ADI): Influence of austempering temperature on microstructure, mechanical and wear properties and energy consumption. *Metals* **8**:53, 2018. doi:10.3390/met8010053.
- [32] E. Skolek, T. Giętko, W. Swiatnicki, D. Myszk. The comparative study of the microstructure and phase composition of nanoausferritic ductile iron alloy using SEM, TEM, magnetometer, and X-ray diffraction methods. *Acta Physica Polonica A* **131**:1319 – 1324, 2017. doi:10.12693/APhysPolA.131.1319.
- [33] A. Basso, M. Caldera, J. Sikora. Mechanical characterization of dual phase austempered ductile iron. *Isij International - ISIJ INT* **50**:302 – 306, 2010. doi:10.2355/isijinternational.50.302.
- [34] M. Palm. Concepts derived from phase diagram studies for the strengthening of Fe–Al-based alloys. *Intermetallics* **13**(12):1286 – 1295, 2005. doi:10.1016/j.intermet.2004.10.015.
- [35] D. Connetable, J. Lacaze, P. Maugis, B. Sundman. A calphad assessment of Al–C–Fe system with the κ carbide modelled as an ordered form of the fcc phase. *Calphad* **32**(2):361 – 370, 2008. doi:10.1016/j.calphad.2008.01.002.
- [36] A. Shayesteh-Zeraati, H. Naser-Zoshki, A. Kiani-Rashid. Microstructural and mechanical properties (hardness) investigations of Al-alloyed ductile cast iron. *Journal of Alloys and Compounds* **500**(1):129 – 133, 2010. doi:10.1016/j.jallcom.2010.04.003.
- [37] V. Di Cocco, D. Iacoviello, F. Iacoviello, A. Rossi. Graphite nodules influence on DCIs mechanical properties: experimental and numerical investigation. *Procedia Engineering* **109**:135 – 143, 2015. doi:10.1016/j.proeng.2015.06.223.
- [38] A. Kiani-Rashid. Influence of austenitising conditions and aluminium content on microstructure and properties of ductile irons. *Journal of Alloys and Compounds* **470**(1):323 – 327, 2009. doi:10.1016/j.jallcom.2008.02.070.
- [39] R. Abbaschian, L. Abbaschian, R. E. Reed-Hill. *Physical Metallurgy Principles*. Cengage Learning, Stamford, USA, 4th edn., 2009.
- [40] ASTM E112-12 - Standard Test Methods for Determining Average Grain Size. Standard, American Society for Testing and Materials, West Conshohocken, 2012.
- [41] ISO 1083-05 - Spheroidal graphite cast irons – Classification. Standard, International Organization for Standardization, Geneva, 2005.